Performance of SAGECal calibration

Kohei Kumazaki[1], Sarod Yatawatta[2] and Saleem Zaroubi[3]
[1]Nagoya University, Furo-cho, Chikusa-ku, Nagoya 464-8601, Japan; kumazaki@a.phys.nagoya-u.ac.jp
[2]ASTRON, Postbus 2, 7990 AA Dwingeloo, The Netherlands; yatawatta@astro.nl
[3]Kapteyn Astronomical Institute, University of Groningen, The Netherlands; saleem@astro.rug.nl

Abstract

In this paper, we investigate the accuracy of SAGECal calibration using real models of the sky for the North Celestial Pole (NCP) and 3C196 windows, and compare the results between these two sky models in order to determine a suitable sky window for Epoch of Reionization (EoR) signal detection. The 3C196 window has a bright source at the phase center and many weak sources around it. The NCP window does not have such a bright source, but have only weak sources. The accuracy for estimation of foreground effect for the case of 3C196 is better than that of NCP due to its high signal to noise ratio. On the other hand, residuals after removal of foreground in the real space for 3C196 are higher due to its brightness. According to these results, we conclude that NCP sky window can provide more accurate removal of foregrounds, and 3C196 sky window can provide more accurate estimation of sky noise effect which includes ionospheric and beam effects.

I. Introduction

The detection of signals from the Epoch of Reionization (EoR) is a very challenging task due to the need for removing huge foreground contamination's which hide the sought after signal. Therefore, accurate calibration accomplishing the removal of foreground contamination is needed.

As crucial aspects of calibration, two issues can be considered. First one is accuracy since the signal from EoR is so weak compared with foreground. In fact, the amplitude of foreground emission is higher by 4–5 orders of amplitude of the EoR signal in the frequency range for EoR experiment [1]. Therefore the foreground removal must be careful and rigorous. Second one is computational cost because of the need to process huge amounts of data. Calibration is basically the Maximum Likelihood (ML) estimation of all components of sky and instrumental systematic errors and calibration is performed using iterative techniques such as the Levenberg–Marquardt [2], [3] algorithm (LMA) or trust region methods [4]. Therefore, the computational cost is much higher compared with a linear estimation problem.

The Space Alternating Generalized Expectation Maximization (SAGE) algorithm [5], [6], [7] is one of the improved methods for calibration, which gives not only lower computational cost but also faster convergence speed than traditional calibration. Even if we use the calibration method which has lower computational cost, however, the time needed for data analysis is still bigger because of huge amount of data. Therefore, by knowing the better sky window to observe to extract the EoR signal, we can cut down significant amounts of observing time.

In order to do this, we have done extensive simulations of the NCP and 3C196 windows where we have simulated interferometric observations for LOFAR telescope. Realistic sky models were used and errors due to ionosphere and beam shape were simulated. Finally, we have used SAGECal to perform calibration of these observations and analyzed the results.

II. Simulation and Calibration

The details of the observational parameters used in the simulation is given in Table I. In Fig. 1, we show the sky models used in the simulations. Note that we have simulated more sources than what we use in calibration. The weak sources not included in calibration also act as an additional source of noise [8].

Assume that we observe K radio sources by a radio interferometer which has N antennas for both skies. Each antenna p receives fully polarized signals from each source which have two orthogonal polarization feeds $\vec{e}_i = [e_X, e_Y]_i^T$ as well. The

		NCP	3C196
Phase center	R.A.	00:00:00.000	08:13:36.0678
	Dec.	+90.00.00.000	+48.13.02.5810
Frequency	MHz	150	
Number of stations		61	
Number of baselines		1830	
Longest baseline	km	$\sim$70	$\sim$80
Observing time	hours	8	
Integration time	sec	10	
Number of time samples		2876	

TABLE I. Details of NCP and 3C196 sky windows

978-1-4673-5225-3/14/$31.00 ©2014 IEEE

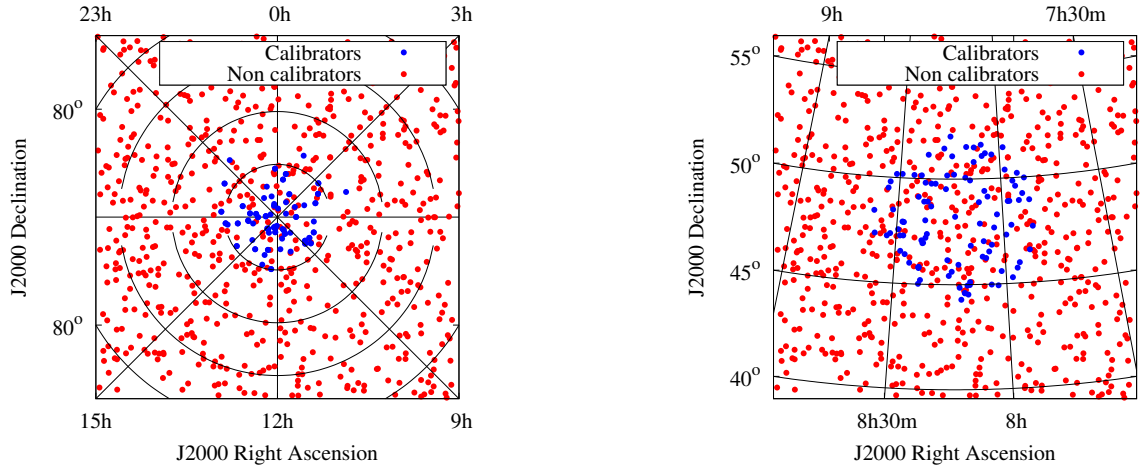

(a) (b)

Fig. 1. Sources in the (a) NCP and (b) 3C196 windows. Sources that are included in the calibration as well as additional sources are shown.

induced voltage at each antennas can be written by

$$\vec{v}_p = \sum_{i=1}^{K} \mathbf{J}_{pi}\vec{e}_i + \vec{n}_p, \tag{1}$$

where the 2×2 Jones matrices $\mathbf{J}_{pi}$ represents the contamination by sky noise or instrumental noise and $\vec{n}$ represents the measurement noise. After that, we need to take correlation between each two antennas, since each voltage has geometric delay depending on the location of the antennas on the earth. Because the each signal are uncorrelated, the correlated voltages between p-th antenna and q-th antenna, called as visibility, is written by

$$\mathbf{V}_{pq} = \sum_{i=1}^{K} \mathbf{J}_{pi}\mathbf{C}^i\mathbf{J}_{qi}^H + \mathbf{N}_{pq}, \tag{2}$$

where $\mathbf{C}^i \equiv E\{\vec{e}_i \otimes \vec{e}_i^H\}$ is the coherency matrix which provides us the polarization information of the i–th source. Then, the vectorized formula of Eq. (2) can be written as,

$$\mathbf{v}_{pq} = \mathrm{vec}(\mathbf{V}_{pq}) = \sum_{i=1}^{K} \mathbf{J}_{qi}^* \otimes \mathbf{J}_{pi}\,\mathrm{vec}(\mathbf{C}^i) + \mathrm{vec}(N_{pq}) \tag{3}$$

Ignoring the auto-correlations, $p = q$, and stacking up all cross-correlations as $\mathbf{y} = [\mathbf{v}_{12}^T, \mathbf{v}_{13}^T, \ldots, \mathbf{v}_{(N-1)N}^T]$. Then the measurement equation can be written as

$$\mathbf{y} = \sum_{i=1}^{K} \mathbf{s}_i(\theta) + \mathbf{n}, \qquad \mathbf{s}_i(\theta) \equiv \begin{bmatrix} \mathbf{J}_{2i}(\theta)\,\mathbf{C}^i\,\mathbf{J}_{1i}^H(\theta) \\ \mathbf{J}_{3i}(\theta)\,\mathbf{C}^i\,\mathbf{J}_{1i}^H(\theta) \\ \vdots \\ \mathbf{J}_{Ni}(\theta)\,\mathbf{C}^i\,\mathbf{J}_{(N-1)i}^H(\theta) \end{bmatrix}. \tag{4}$$

The number of elements in $\mathbf{y}$ and $\mathbf{n}$ is at least $2N(N-1)$.

We have simulated the values of $\mathbf{J}_{pi}$ for all p,i to model realistic ionospheric and beam errors. We have also added noise. Afterwords, we have calibrated the data (only along the directions of the calibrators) using SAGECal. The details of the calibration algorithms can be found in [6], [7], [8].

III. Comparison NCP window with 3C196 window

In this section, we compare error level after SAGECal calibration for both sky models. In order to do that, we define three errors. We show the comparison of errors between NCP and 3C196 window in Fig. 2.

1) **Error in Jones matrices** First one is the error between estimated Jones matrices and input Jones matrices. That can be calculated as the subtractions between input Jones matrices and estimated Jones matrices (after removing unitary ambiguities [9]) and normalized mean square error (NMSE) which is written by

$$\mathrm{NMSE}_i \equiv \frac{1}{N}\sum_{p=1}^{N}\frac{||\,\mathrm{J}_{pi}-\tilde{\mathrm{J}}_{pi}\,||^2}{||\mathrm{J}_{pi}||^2}\ . \tag{5}$$

The left top panel of Fig. 2 shows NMSE. We find that stronger sources basically provide more accurate (small variance) solutions. That is because stronger sources have higher SNR. According to this strategy and looking at upper left panel, estimation of Jones matrices for NCP is at least 10 times larger than 3C196 window, of course, because of lower SNR. It means that 3C196 window is better to study the effects contained in Jones matrices.

2) **Error along the direction of calibrators** Second one is the residual in the image space after SAGECal for each calibrators. Since SAGECal removes the calibrators in the uv-space, we have to make images (using `casa`). Then we measure the intensities at each source position, $\hat{\mathbf{C}}_i$ and calculate percentage of residuals which is written by

$$\text{on source error}_i = \frac{\hat{\mathbf{C}}_i}{\mathbf{C}_i}\times 100 \quad [\%]\ . \tag{6}$$

Focusing on the on source error shown at left bottom panel in Fig. 2, the ratio of removed intensity for 3C196 is also smaller than NCP (see in lower panel of bottom panel in Fig. 2) due to better estimation of Jones matrices. However, averaged residual value for 3C196 is roughly few times larger than NCP because of its brightness.

3) **Off–source error** Third one is also the residuals on the real space images after SAGECal but directions away from calibrators. This error describes the removal error of leakage from calibrators due to sky noise and instrumental noise. Hence, we measure the intensity along a direction which any calibrator does not exist and make a histogram of intensities. The variance of this histogram is called off source error. We treat these three errors as an indicator of accuracy.
We show the off source error at right in Fig. 2 by histograms. Upper panel describes the case of NCP. The histogram with black line represents the input measurement noise on the map which has σ_n^2 = 1 mJy/pixel. Red unshaded spread histogram is the noise on the map before calibration which is roughly twice larger than measurement noise because of leakage from calibrators. Then the red shaded histogram which do completely correspond to the black one is the noise after calibration. For NCP, the leakage from extragalactic foreground can be removed at least lower than measurement noise level. On the other hand, the blue unshaded histogram in right lower panel of Fig. 2 has slightly larger variance than black histogram. It means that the leakage in the case of 3C196 can be hardly removed due to large contamination from the brightest calibrator which can be seen as a few ten times larger noise than measurement noise (see blue unshaded histogram in the right lower panel of Fig. 2).

According to the on source error and off source error, NCP window seems to be better to eliminate extragalactic foreground and leakage. This fact means that it is better suited for us to study background emission, such as signals from reionization epoch.

REFERENCES

[1] V. Jelic, S. Zaroubi, P. Labropoulos, R. M. Thomas, G. Bernardi, M. A. Brentjens, A. G. De Bruyn, B. Ciardi, G. Harker, L. V. E. Koopmans, V. N. Pandey, J. Schaye, and S. Yatawatta, "Foreground simulations for the lofarepoch of reionization experiment," *Monthly Notices of the Royal Astronomical Society*, vol. 389, no. 3, pp. 1319–1335, 2008.

[2] K. Levenberg, "A method for the solution of certain non linear problems using least squares," *The Quarterly Jnl. of App. Math.*, vol. 2, pp. 164–168, 1944.

[3] D. Marquardt, "An algorithm for least squares estimation of nonlinear parameters," *SIAM Jnl. of App. Math.*, vol. 11, pp. 431–441, 1963.

[4] S. Yatawatta, "Radio interferometric calibration using a riemannian manifold," in *Acoustics, Speech and Signal Processing (ICASSP), 2013 IEEE International Conference on*, 2013, pp. 3866–3870.

[5] J.A. Fessler and A.O. Hero, "Space alternating generalized expectation maximization algorithm," *IEEE Trans. on Sig. Proc.*, vol. 42, no. 10, pp. 2664–2677, Oct. 1994.

[6] S. Yatawatta, S. Zaroubi, G. de Bruyn, L. Koopmans, and J. Noordam, "Radio interferometric calibration using the SAGE algorithm," *in proc. 13th IEEE DSP workshop*, pp. 150–155, Jan. 2009.

[7] S. Kazemi, S. Yatawatta, S. Zaroubi, P. Labropoluos, G. de Bruyn, L. Koopmans, and J. Noordam, "Radio interferometric calibration using the SAGE algorithm," *MNRAS*, vol. 414, no. 2, pp. 1656–1666, June 2011.

[8] S. Kazemi and S. Yatawatta, "Robust radio interferometric calibration using the t-distribution," *Monthly Notices of the Royal Astronomical Society*, vol. 435, pp. 597–605, Oct. 2013.

[9] S. Yatawatta, "On the interpolation of calibration solutions obtained in radio interferometry," *Monthly Notices of the Royal Astronomical Society*, vol. 428, pp. 828–833, Jan. 2013.

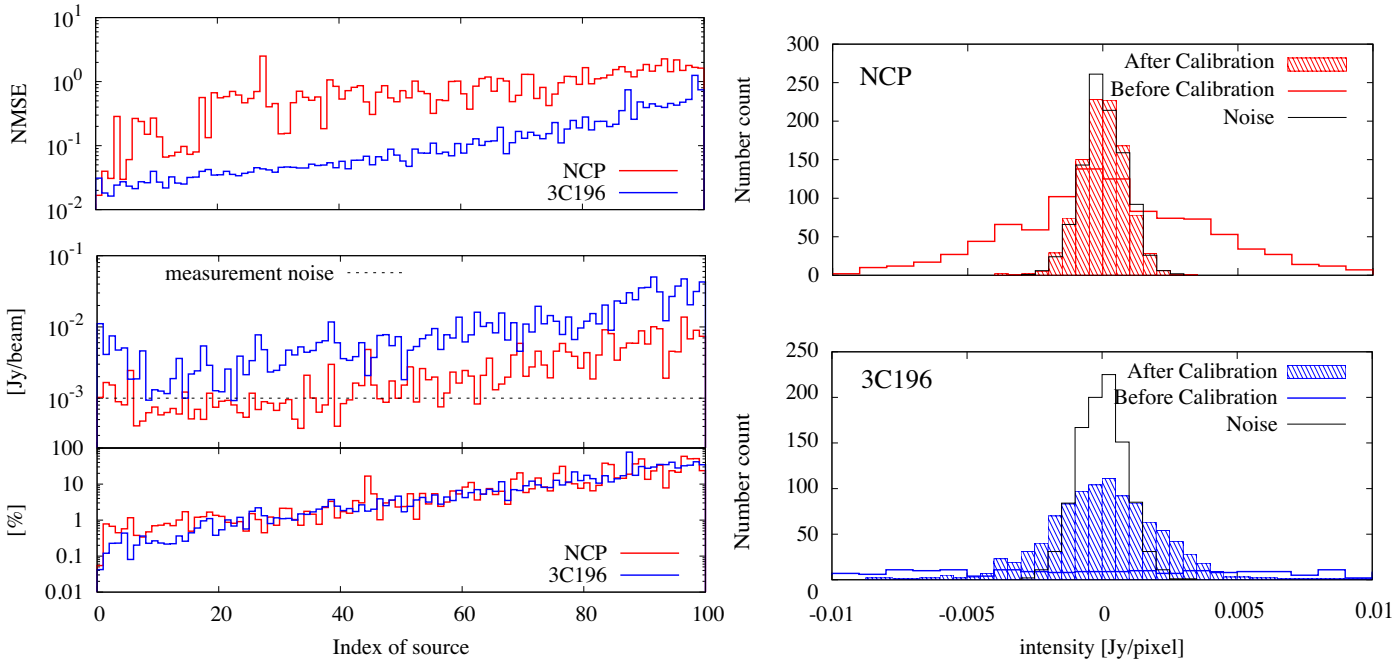

Fig. 2. Left panels: The comparison the error of NCP (red line) with 3C196 (blue line). Upper and lower panel show the NMSE and the on source error. Right panels: The comparison of the noise on the map. Top and bottom panel describe the case of NCP and 3C196. Black line represents the input noise. Shaded and unshaded histogram shows the noise on the map before and after calibration, respectively. Broad unshaded histogram is caused by the leakage from extragalactic foreground due to sky and instrumental noise.